Appl Phys B (2012) 106:707–715
DOI 10.1007/s00340-012-4903-2

Applied Physics B
Lasers and Optics

Effect of hydrogen addition on soot formation in an ethylene/air premixed flame

S. De Iuliis · S. Maffi · F. Migliorini · F. Cignoli · G. Zizak

Received: 12 October 2011 / Revised version: 28 December 2011 / Published online: 7 February 2012

Abstract The effect of hydrogen addition to fuel in soot formation and growth mechanisms is investigated in a rich ethylene/air premixed flame. To this purpose, three-angle scattering and extinction measurements are carried out in flames with different hydrogen contents. By applying the Rayleigh–Debye–Gans theory and the fractal-like description, soot concentration and morphology, with the evaluation of radius of gyration, volume-mean diameter and primary particle diameter are retrieved. To derive fractal parameters such as fractal dimension and fractal prefactor to be used for optical measurements, sampling technique and TEM analysis are performed. In addition, data concerning soot morphology obtained from TEM analysis are compared with the optical results. A good agreement in the value of the primary particle diameter between optical and ex-situ measurements is found. Significant effects of hydrogen addition are detected and presented in this work. In particular, hydrogen addition to fuel is responsible for a reduction in soot concentration, radius of gyration and primary particle diameter.

Nomenclature

a	primary particle radius
A_a	projected area of aggregate
A_p	projected area of primary particle
$[C]_{soot}$	carbon atom concentration in soot
$[C]_{tot}$	carbon atom concentration in the initial mixture
D_{30}	volume-mean diameter
D_f	fractal dimension
d_p	primary particle diameter
$E(m)$	function of soot refractive index m for absorption
f_v	soot volume fraction
k_a	projected area constant
k_f	fractal prefactor
k_L	correlation constant
I_0	incident laser beam intensity
I_ℓ	emerging laser beam intensity
ℓ	light path length
N	number of primary particles within an aggregate
N_{av}	Avogadro number
R_g	radius of gyration of an aggregate
R_L	outer radius of an aggregate
χ_{soot}	soot conversion efficiency

Greek Symbols

α	projected area exponent
λ	wavelength of light source
ρ	soot particle density

1 Introduction

Recent research and development in the area of combustion have been motivated by commitments of preserving a clean environment and reducing energy consumption. In the recent past, hydrogen has received attention as a potential alternative for fossil fuel based power generation. From a combustion point of view, hydrogen possesses superior characteristics to any hydrocarbon fuel in terms of ignitability, low ignition delay, and higher flame stability. However, its higher flammability and lower volumetric density make the on-board storage system complicated for transportation and power generation. As an intermediate solution, hydrogen-hydrocarbon hybrid fuels have received increasing attention

S. De Iuliis (✉) · S. Maffi · F. Migliorini · F. Cignoli · G. Zizak
CNR-IENI, Istituto per l'Energetica e le Interfasi,
Sede di Milano via Cozzi 53, 20125, Milano, Italy
e-mail: deiuliis@ieni.cnr.it
Fax: +39-02-66173321

since they improve combustion performance, both in terms of combustion ignitability and stability and in terms of pollutants emission reduction (NO_x and soot). It is clear that the change of the fuel composition effects both chemical and physical processes occurring in flames [1]. The combustion features of these fuels are difficult to predict due to the complex and nonlinear nature of chemical kinetics and multicomponent diffusion processes. A pioneering work was presented by Tesner in 1958 [2], showing that dilution of natural gas by hydrogen slows down the formation of carbon black particles during thermal decomposition. Most of the studies to follow concerned the effect of hydrogen addition on flame stability, burning velocity, flame structure, and flow field, performed in different combustion systems such as jet diffusion flames [3, 4], swirled turbulent diffusion flames [5, 6], laminar diffusion [7], and lean premixed flames [8, 9]. As a result, hydrogen has been shown to cause an extension of the flame stability limits, an increase of the burning velocities, and a significant change in the flame structure and flow field. The effect of hydrogen addition on pollutant emission has mainly been investigated numerically. Tseng [10] numerically investigated the effect of hydrogen addition on premixed combustion of methane in a porous medium burner, showing that CO emission increases slightly as the hydrogen fraction in the fuel is raised. Ilbas et al. [11] performed a numerical simulation of a turbulent non-premixed hydrogen flame in a model combustor. These last studies were carried out changing fuel composition from pure hydrogen to natural gas. The results showed that the overall flame temperature increases as hydrogen is added, resulting in an increase in NO_x emission as well.

The work by Gülder et al. [1] is one of the few experimental investigations focused on the effects of hydrogen and helium addition to the ethylene flame on soot formation. Recently, Guo et al. [12] numerically investigated the same combustion system using a detailed reaction mechanism. Their results were in good agreement with [1]. The relative influence of dilution and direct chemical interaction on soot formation was studied by comparing the results obtained with hydrogen addition with the ones obtained with helium addition. Results in [1] showed that hydrogen is more effective than helium in suppressing soot formation when added to ethylene. Such higher effectiveness is not found for additions to propane or butane. By observing that blending hydrogen or helium does not significantly alter the temperature distribution, or the visible flame height, they argued that the greater effectiveness of hydrogen addition to ethylene compared to that of helium addition is due to the chemical effect of hydrogen. Similarly, Du et al. [13] found that hydrogen addition on ethylene, propane, and butane substantially reduces the soot inception strain rate. Their results also indicate that the addition of helium to fuel is more effective than hydrogen in suppressing soot formation, despite the higher flame temperature that results from hydrogen addition.

Much work is still required for a deeper understanding of the physical-chemical mechanisms behind the combustion of these hybrid fuels in different experimental conditions.

In this work, the influence of hydrogen addition to fuel on soot formation is investigated in a premixed ethylene/air flat flame using laser diagnostic techniques. Three-angle scattering coupled with light extinction is applied. Parameters concerning the soot load, such as soot volume fraction and soot conversion efficiency as well as soot morphology, with the evaluation of the radius of gyration and of the primary particle diameter, are presented for flames with different hydrogen content. Transmission Electron Microscope (TEM) analysis is also performed. Considering a fractal-like description, soot fractal parameters such as fractal dimension and fractal prefactor are obtained by analyzing TEM soot micrographs. These parameters are used in the numerical approach for soot characterization by scattering measurements. To better characterize combustion processes and soot formation mechanisms temperature measurements are also performed. Moreover, TEM results on soot sizing are compared with the ones retrieved with optical measurements.

2 Scattering/extinction—basic approach

The three-angle scattering/extinction technique has been widely described in [14, 15], following the methodology outlined in [16]. Here, only the main relationships are reported.

According to the Lambert–Beer's law, from the monochromatic transmittance and the extinction coefficient, the soot volume fraction (f_v) of a homogeneous medium is evaluated using the relationship [14]:

$$f_v = \frac{-\ln(\frac{I_\ell}{I_0})\lambda}{6\pi \ell E(m)} \tag{1}$$

where I_ℓ and I_o are the emerging and incident laser beam intensity, λ is the wavelength of the probe beam; ℓ is the path length of the homogeneous medium producing the extinction and $E(m)$, that is related to the soot absorption coefficient (K_{abs}) [14], is a function of the real, n, and imaginary, k, part of the refractive index m ($m = n - ik$).

Soot morphology was investigated by applying the approach reported in [14], where the fractal-like description is combined with the Rayleigh—Debye–Gans (R-D-G) theory and the three angle scattering and extinction measurements.

According to the mass fractal approximation, the relationship between the primary particle diameter, d_p, and the number of these particles within an aggregate, N, is given by [17]:

$$N = k_f (R_g/d_p)^{D_f} \tag{2}$$

where R_g is the radius of gyration of an aggregate, D_f is the fractal dimension, and k_f is a fractal prefactor, for which

different values are reported in several works (e.g., $D_f = 1.7–1.9$ [18, 19]; $k_f = 5.8$ [19], 8.5 [20], and 9.4 [21]).

These fractal parameters are retrieved from TEM measurements as reported in Sect. 4.1, while to determine the primary particle diameter d_p, the mean value of the radius of gyration R_{gm1} and the volume-mean diameter D_{30} have to be evaluated. The mean value of the radius of gyration is defined as follows:

$$R_{gm1} = d_p(\overline{m_1}/k_f)^{(1/D_f)} \tag{3}$$

with a mean number of primary particles in the aggregate $\overline{m_1}$, and is obtained from the dissymmetry ratio, $R_{VV}(\theta_1, \theta_2)$, which is defined as the ratio between the vertically polarized scattering signals detected at two scattering angles, θ_1 and θ_2 [14]. The volume-mean diameter is derived by ratioing the scattering coefficient measured at 90° and the extinction coefficient.

Then soot primary particle diameter is obtained as

$$d_p^{3-D_f} = \frac{D_{30}^3}{k_f R_{gm1}^{D_f}} \tag{4}$$

3 Experimental set-up

The experimental apparatus used for scattering/extinction measurements is the same as the one reported in [14] and is here briefly recalled. A McKenna burner (Holthuis and Associates) with a bronze porous plug is used to produce premixed "flat" flames [22]. The flame is shielded with a flow of Nitrogen (Sapio, 99.99% purity) and stabilized with a stainless steel plate located 20 mm above the burner surface. The flow rates of fuel and oxidizer are measured and controlled using calibrated mass flow meters (Bronckhorst, AK Ruurlo, Netherlands).

For scattering measurements, the vertically polarized green beam (514 nm wavelength) of a CW Ar^+Kr^+ laser (Coherent Innova 70C spectrum), kept at 200 mW output, is used. The beam is interrupted by a mechanical chopper (frequency 300 Hz) and focused on the burner axis with an 800 mm focal length lens. To detect the scattering signal at different angles, the burner is placed at the center of a goniometric rolling platform holding the receiving optics. The light scattered from the probe volume is collected and focused onto a 1 mm wide slit placed in front of the photomultiplier tube (Hamamatsu R4220). To detect only the vertically polarized component of the scattering signal at the laser wavelength an interference filter ($\lambda = 514$ nm, $\Delta\lambda = 1$ nm) and a polarizer plate are used. The signal is processed with a digital lock-in amplifier (Stanford Research Systems, model SR850 DSP) coupled with the mechanical chopper to discriminate the scattered light against flame emission. Scattering signals are collected at 30°, 90°, and 150°. To derive the soot scattering coefficient, a calibration procedure is carried out using nitrogen and methane, whose scattering cross sections are known. For extinction measurements, the 1064 nm beam of a CW Nd:YAG laser (Changchun New Industries Optoelectronics, Changchun China, model DPSSL, 10 mW) is focused on the flame axis and the transmitted beam directed into an integrating sphere, which allows to avoid beam steering due to thermal gradients at the flame edges. The intensity signal is measured with a photomultiplier tube (Hamamatsu H5783-01) and processed by means of the same digital Lock-in amplifier used for scattering measurements. The acquisition of both scattering and extinction measurements is driven by a personal computer. To improve the signal to noise ratio, each signal results from an average of 300 samples.

Soot samples were collected using thermophoretic sampling for TEM analysis. The probe, consisting of a TEM grid (Cu with carbon film, $\phi = 3$ mm, TAAB) and a stainless steel holder, was rapidly inserted into the flame by a double-action electro-pneumatic system. The residence time inside the flame was 50 ms.

Soot samples were collected at the flame axis 10 mm and 14 mm height above the burner (HAB) and analyzed with a Transmission Electron Microscope (TEM, Jeol Jem 2000 FXII). Digital TEM micrographs collected with a CCD camera (Olympus, 1376 × 1032 pixels) were processed using iTEM Olympus software.

Temperature measurements were also performed along the flame axis using a 50 μm Pt/Pt-Rh(10%) uncoated thermocouple and were corrected for heat losses [23]. The shielding effect due to the deposition of soot particles on the thermocouple junction, resulting in a underestimation of the temperature, was overcome according to the procedure reported in [24, 25].

The investigation was carried out on an ethylene/air laminar premixed flame at atmospheric pressure (equivalence ratio 2.3) with the addition of two different hydrogen concentrations. In Table 1, details about the reactant gases are given. Hydrogen-doped flames are obtained by replacing a certain amount of ethylene in the flame A with a corresponding amount of hydrogen, then adjusting the air flow rate to keep constant the following parameters: total flow rate (10 Nl/min), cold gas flow velocities (5.84 cm/s), and C/O ratio (0.775). In this work, 20% and 40% of hydrogen volumetric flow with respect to the ethylene volumetric flow (Table 1) are investigated.

As a consequence of the changing composition, a corresponding variation in the equivalence ratio for the three cases under study is obtained as shown in the table. In the same table, adiabatic temperature values obtained from thermodynamic calculations are also reported. As it can be observed, by adding hydrogen to the mixture only a slight decrease in the adiabatic temperature is calculated, being about 50 K with 40% H_2.

Table 1 Experimental conditions of the flames under study. T_{ad} is the adiabatic flame temperature

flame #	C_2H_4 [Nl/min]	H_2 [Nl/min]	$H_2/C_2H_4 * 100$	Air [Nl/min]	Φ	T_{ad} (K)
A	1.40	0	0	8.60	2.3	1736
B	1.36	0.272	20	8.34	2.5	1711
C	1.33	0.531	40	8.14	2.7	1680

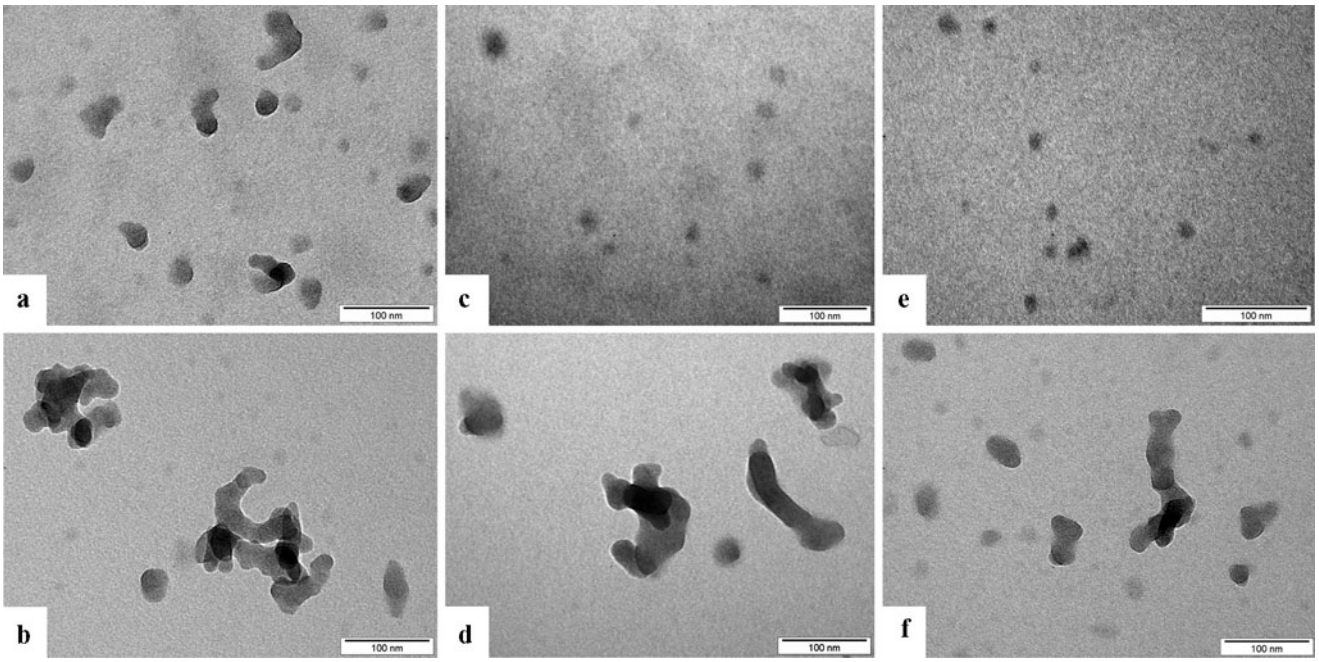

Fig. 1 TEM micrographs of soot samples collected at HAB = 10 mm (*top*) and 14 mm (*bottom*) in the pure ethylene/air flame ((**a**), (**b**)), with 20% H_2 addition ((**c**), (**d**)) and with 40% H_2 addition ((**e**), (**f**)), respectively

4 Results and discussion

4.1 TEM measurements

In Fig. 1, measurements carried out at HAB = 10 mm and 14 mm for the three flames A (0% H_2), B (20% H_2), and C (40% H_2) are shown. Considering the nondoped case, the same observation already reported in [14] can be made. Well-defined aggregates are present at HAB = 14 mm, in which contrasted individual particles can be discriminated. On the contrary, at HAB = 10 mm the aggregation is less significant and the particles present a faint and poorly defined contour. The objects observed at this height above the burner are translucent (almost transparent to the electron beam) and exhibit a liquid-like behavior. The features at this height can be attributed to the presence of young soot particles, which are characterized by different physical and chemical properties with respect to mature soot. This observation is in agreement with previous measurements reported in the literature [26, 27].

It is interesting now to observe the role of hydrogen addition on soot morphology. By increasing hydrogen content, aggregation processes are less significant (HAB = 14 mm) and the presence of translucent objects with features of transparency and liquid-like behavior is more pronounced (HAB = 10 mm).

To highlight these features, an interesting observation by TEM can be performed by looking at the edge of a broken carbon film, which allows a kind of three-dimensional visualization of the structures.

In Fig. 2, three images collected at HAB = 10 mm and in two different flames are reported. In particular, the first two images have the same magnification and refer to the case of pure ethylene/air flame (Fig. 2a) and the one with 20% H_2 addition (Fig. 2b), whereas the Fig. 2c is a micrograph collected still in the 20% H_2 addition flame, but with a higher magnification and a different view angle due to the slanting edge of the carbon film. The features of the structures are here more evident, and the particular visualization makes clearer their liquid-like nature. This observation allows to infer that at HAB = 10 mm it is difficult to measure soot particle diameter without any overestimation of the results. Moreover, with increasing hydrogen content, such measurements are more difficult as the faint and

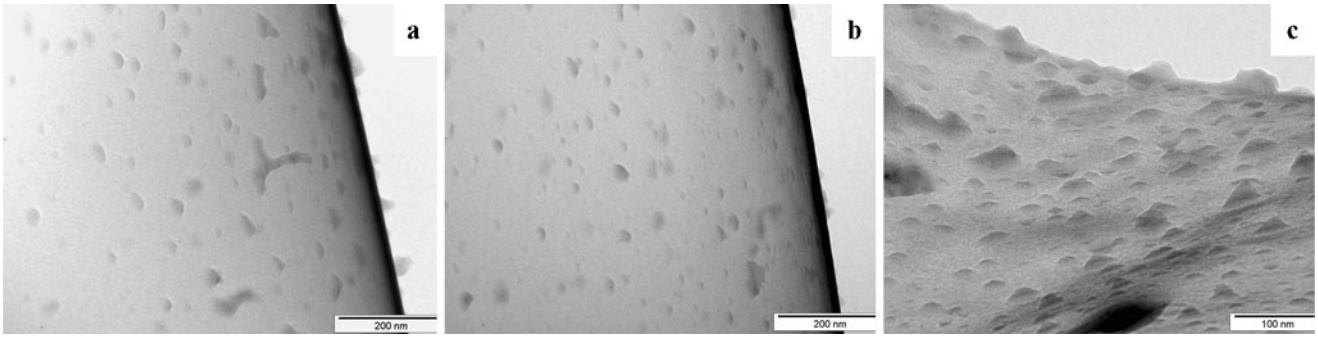

Fig. 2 TEM images close to the edge of a broken carbon film inside the grid mesh at HAB = 10 mm: (**a**) 30 kx, no hydrogen-doped flame; (**b**) 30 kx, 20% H_2 addition, and (**c**) 50 kx, 20% H_2 addition

translucent nature of such objects becomes more marked. Therefore, the quantitative analysis of the TEM soot micrographs has been carried out only at the height of 14 mm for all the flames under study. Soot parameters such as primary particle size, geometric aggregate dimensions, fractal dimension D_f, and fractal prefactor k_f are retrieved. The values of D_f and k_f (obtained at HAB = 14 mm) are then used in the scattering/extinction approach to derive soot parameters at any height above the burner. In fact, as reported in a previous work [14], in regions with abundant presence of mature soot particles, the values of the fractal parameters exhibit no significant differences with the height above the burner. On the contrary, a meaningful change in the fractal values is observed in the presence of young soot.

A comparison of TEM parameters related to the soot size and morphology with the results obtained with the scattering/extinction measurements is then performed.

The analysis of soot samples is carried out on the projected images of a set of aggregates following the procedure described in [20]. For soot particle diameter, due to the uncertainty in measuring particles contour, about 300 particles were analyzed for the pure ethylene/air flame and for the one with 20% H_2 addition, while only about 100 for the 40% H_2 flame. Especially in the last case, in fact, most of the spots were very blurred and, therefore, discarded in order to avoid large subjective errors. The primary particle size distribution resulted to be very narrow, therefore, hereafter we refer to an average value of the soot diameter (weighted mean).

Similarly, fractal parameters were derived from a set of about 300 aggregates in the pure flame and in 20% H_2 addition, whereas about 100 in 40% H_2 addition.

For each aggregate, the maximum Feret length and the aggregate projected area (A_a) are measured. This area together with the mean primary particle cross section A_p allows to derive the number of particles in an aggregate [20] as follows:

$$N = k_a \left(\frac{A_a}{A_p} \right)^{\alpha} \tag{5}$$

where k_a and α are empirical constants; from the literature it was found $k_a = 1.15$ and $\alpha = 1.09$ [20].

For the three flames, at HAB = 14 mm, the analysis indicates the presence of clusters with a polydisperse number of primary particles per aggregate well described by a log-normal function. The standard deviation of the probability distribution is $\sigma = 2.1$ for the nondoped flame, and 2.5 and 2.4 for 20% and 40% H_2 addition, respectively.

The outer radius of an aggregate R_L (the half of the maximum Feret length) is related to the particle radius, a, according to the following relationship:

$$N = k_L \left(\frac{R_L}{a} \right)^{D_f} \tag{6}$$

where k_L is the correlation constant that is related to the fractal prefactor [20]. Reporting the logarithm of N vs. the logarithm of R_L/a a linear trend is obtained. The slope gives the fractal dimension and the intercept is the logarithm of the correlation constant. By comparing (6) with the (2) k_f can be derived as follows:

$$\frac{k_f}{k_L} = 2^{D_f} \left(\frac{R_L}{R_g} \right)^{D_f} \tag{7}$$

where the radius of gyration is evaluated with the following relationship [28, 29]:

$$\left(\frac{R_L}{R_g} \right) = \left[\frac{(D_f + 2)(D_f + 5)}{2D_f(D_f + 1)} \right]^{1/2} \tag{8}$$

This equation is obtained using the cut-off function proposed in [28] which is related to the density autocorrelation function.

In Fig. 3, the results obtained for the three flames are shown. For each flame, the linear fitting curve and the corresponding analytical expression are also reported. In all cases, a good correlation is obtained, as indicated by the values of the coefficient of determination, R^2, which confirms the fractal behavior of these structures even in the case of 40% H_2 addition.

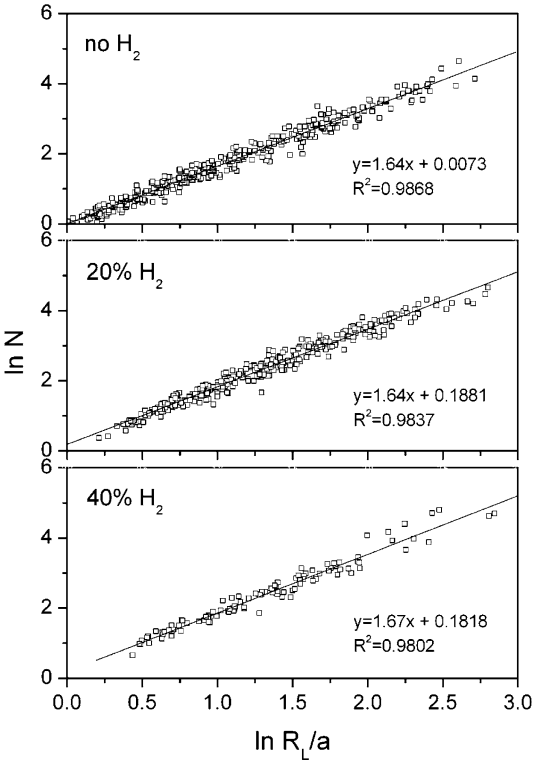

Fig. 3 The logarithm of the number of primary particles in each aggregate versus the logarithm of R_L/a of soot collected at HAB = 14 mm for the three flames under study

Table 2 Parameters obtained from TEM analysis for the three flames at HAB = 14 mm

% H2	TEM d_p, nm	σ	D_f	K_f
0	23.01	2.1	1.64	6.04
20	19.67	2.5	1.64	7.24
40	15.62	2.4	1.67	7.39

In Table 2, the fractal parameters obtained for the three different flames are shown, where σ is the standard deviation for R_g of the polydisperse set of aggregates.

The fractal dimension remains constant for the three flames indicating that soot particulate exhibits the same aggregation level. On the contrary, the value of the fractal prefactor slightly increases with hydrogen addition. This behavior can be attributed to an increase in the compactness of the aggregates in doped flames, as suggested by Brasil et al. [30].

4.2 Temperature and scattering/extinction measurements

Temperature measurements were carried out along the flame axis up to HAB = 14 mm with an uncertainty of 50 K and reported in Fig. 4. The curves corresponding to the three flames present a similar trend. Temperature increases rapidly

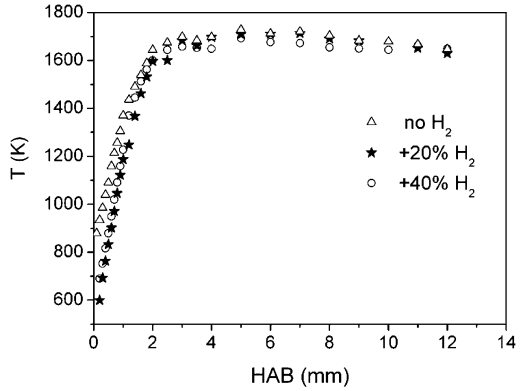

Fig. 4 Temperature measurements versus the height above the burner for the three flames

starting from the burner mouth over the first 2 mm, reaches a maximum and then slightly decreases near the stabilizing plate. The temperatures detected in hydrogen-doped flames are slightly lower than those obtained in the flame without hydrogen, with a maximum difference of about 50 K. The maximum temperature values obtained in the three cases are in agreement with the corresponding adiabatic temperature values reported in Table 1.

In Fig. 5a, soot volume fraction obtained from extinction measurements is reported versus the height above the burner. The measurements are derived using the value of $E_m = 0.29$ at 1064 nm obtained from Laser-Induced Incandescence (LII) measurements [31]. In all cases, a monotonic increase of f_v with HAB is observed. With hydrogen addition a reduction of the soot concentration is detected. It can be observed that, in the case of the pure ethylene/air flame, the maximum f_v is 0.17 ppm detected at HAB = 14 mm. This value corresponds to an absorption coefficient K_{abs} of 0.009 cm^{-1} and an extinction of about 4%. By adding hydrogen to the fuel, a reduction of f_v accounts for a decrease in K_{abs}, and consequently in extinction, which is more significant at low HABs. Therefore, high sensitivity and good signal to noise ratio are required. With the averaging of 300 samples used here, the error in f_v measurements is 3%.

To evaluate the effect of hydrogen addition on soot formation and to take into account the carbon atom concentration in the initial mixture, the conversion of the carbon atom concentration into the one present in the soot particles has to be considered. Provided that a simple comparison between the three flames has to be carried out and that the temperature changes in these systems are verified to be modest, the quantity soot conversion efficiency χ_{soot} is introduced as

$$\chi_{soot} = \frac{[C]_{soot}}{[C]_{tot}} \tag{9}$$

where $[C]_{soot}$ is the carbon atom concentration in the carbonaceous particulate and $[C]_{tot}$ is the same property of the initial mixture. According to Graham's model [32], the soot conversion efficiency can be expressed as

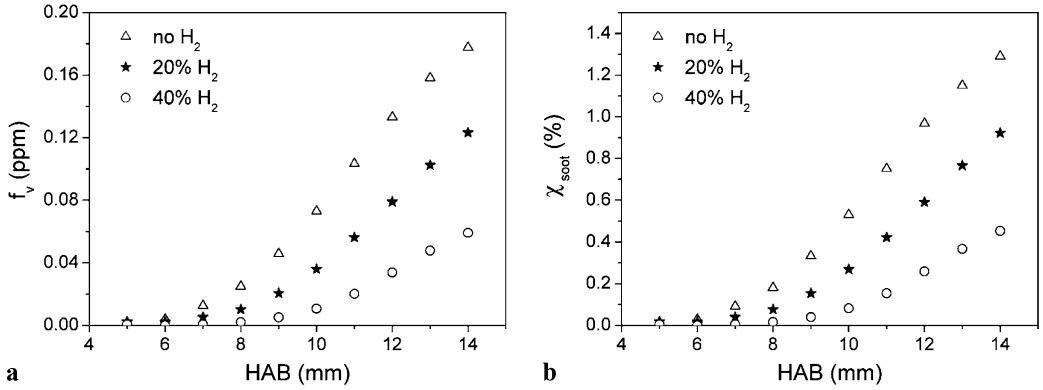

Fig. 5 Axial profile of the soot volume fraction (**a**) and of the soot conversion efficiency (**b**) for the three flames

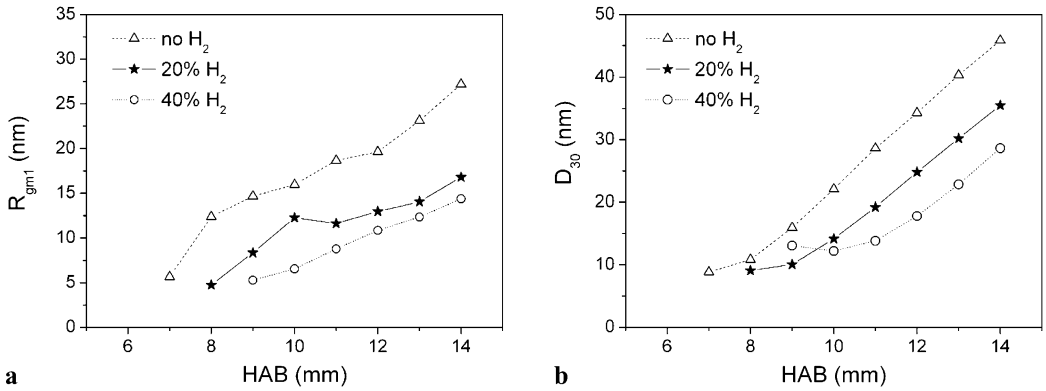

Fig. 6 Average radius of gyration (**a**) and volume-mean diameter (**b**) versus the height above the burner

$$\chi_{\text{soot}} = \frac{N_{\text{av}}\rho}{12[C]_{\text{tot}}} f_{\text{v}} \tag{10}$$

where ρ is the soot particle density (1.8 gr/cm^3) and N_{av} is Avogadro's number.

In Fig. 5b, soot conversion efficiency versus the height above the burner is shown. Since the carbon atom concentration in the initial mixture does not change significantly across the experimental conditions studied, a trend similar to the one obtained for f_{v} is observed.

Both in Fig. 5a and b, by increasing the hydrogen content, the soot inception region shifts higher in the flame. The inception location is found at about HAB = 7 mm for non-doped flame, 8 mm for 20% H_2 flame, and 9 mm for 40% H_2 flame.

From scattering measurements at 30° and 150° and corresponding dissymmetry ratios, the radius of gyration R_{gm1} is derived and its axial profiles reported in Fig. 6a for the three flames. As it is evident in the figure, while a monotonic increase of the radius of gyration with the height is observed in flame C, a change in the slope of the curves is detected for the other two flames. This change is observed at about 8 mm in the flame A, shifted at 10 mm in the flame B, and absent (or not detectable) in the flame C. The behavior observed in the flames A and B suggests the simultaneous occurrence of nucleation and aggregation processes in the inception region.

In Fig. 6b, the axial profiles of the volume-mean diameter are shown. For these measurements, the value of $F(m) = 0.27$ at $\lambda = 514$ nm is used (as proposed in [33] and confirmed in [34]). A reduction of D_{30} is detected by increasing hydrogen content. The slope of the curves is similar for all flames, indicating that hydrogen addition does not affect the growth rate of the volume-mean diameter of soot aggregates. On the contrary, the different trend of the radius of gyration with HAB, already described in Fig. 6a, can be attributed to a competitive occurrence of different aggregation and growth processes involved in soot formation.

In Fig. 7, measurements of soot particle diameter versus the height above the burner are shown. For the three flames, apart from the initial growth region particle diameters exhibit a monotonic increase with the height. Results in the initial growth region can be affected by the difference in the nature, and consequently in the properties, of the young soot particles with respect to mature soot.

It is important to keep in mind, in fact, that the optical soot characterization is obtained using TEM fractal parameters evaluated at HAB = 14 mm and referring to mature

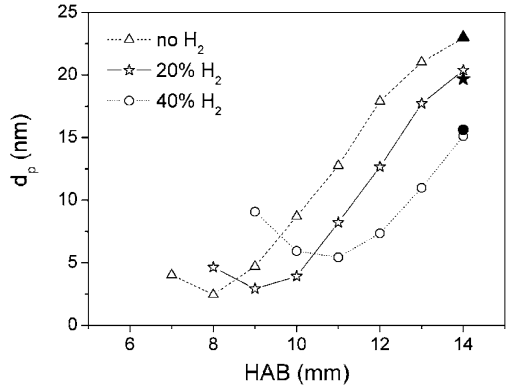

Fig. 7 Primary particle diameter versus the height above the burner. Close symbols are results obtained from TEM image analysis

soot, and so are probably hazardously applicable low in the flame.

Considering the effect of hydrogen on the single particle, a reduction of the size is detected by increasing hydrogen content. In the same figure the value of d_p obtained with TEM measurements (closed symbols) are reported for comparison, confirming a good agreement between the two sets of measurements.

To explain the total behavior of hydrogen addition on such flames, comparisons between all the parameters (temperature (Fig. 4), soot volume fraction (Fig. 5a and b), aggregate radius of gyration (Fig. 6a), volume-mean diameter (Fig. 6b), and soot particle diameter (Fig. 7)) are performed.

As for soot formation, although an increase of the equivalence ratio is obtained with hydrogen addition, the general trend is a total reduction of the particulate, both in terms of volume fraction and in terms of dimension (radius of gyration, volume-mean diameter, and monomers size). Once the change in the carbon atom concentration of the initial mixture (soot conversion efficiency) has been taken into account, keeping C/O ratio constant and since no significant changes in the flames temperature are observed, such reduction can be attributed to the chemical role of hydrogen more than a merely dilution effect.

Even considering the deep differences between premixed and diffusion flames, the results reported here are comfortably paralleled to the ones in [1], in particular concerning the low sensitivity of the temperature field and the general tendency in soot reduction.

The reduction of the carbonaceous particulate can be due to two different parameters that are at the basis of the soot formation process. The first one is the induction delay time necessary to form soot precursors. A longer delay time, and consequently a shorter residual time for precursors to form soot, will lead to a reduction in soot formation. The second parameter is linked to the concentration level of soot precursors (PAH) that can decrease drastically with hydrogen addition, leading to a decrease in the nuclei concentration, and consequently, in the number of particles. Concerning the second hypothesis, the reduction of PAH formation can be explained by the role of H_2 and H radicals in the H-abstraction/C_2H_2-addition reaction mechanism for PAH growth [35]. In fact, according to this model, at high temperature conditions the driving force for PAH growth is the [H]/[H_2] ratio, and as this ratio decreases with the H_2 addition in flame, an inhibition of the chemical PAH growth occurs [35].

Such explanation is also in agreement with previous studies on the chemical effect of H_2 in shock tubes [36].

5 Conclusions

In this work, it is investigated the role of hydrogen addition to fuel in soot formation and growth processes. The investigation is performed in a rich ethylene/air premixed flame with an equivalence ratio of 2.3 and constant C/O ratio of 0.77, at which 20% and 40% H_2 content is added. A full characterization of soot parameters in terms of soot load and morphology is obtained by combining three-angle scattering/extinction measurements and sampling technique for subsequent TEM analysis. Temperature measurements are also carried out.

The effect of hydrogen addition to fuel in our experimental conditions can be summarized as follows:

- the behavior of temperature along the flame is the same for the three flames both in terms of the absolute value and in the axial trend;
- increasing hydrogen addition, a reduction of the soot conversion efficiency is observed along the flame;
- the radius of gyration, the volume-mean diameter and the primary particle diameter decrease significantly with hydrogen addition along the flame;
- hydrogen addition has no effect on the growth rate of the volume-mean diameter, while strongly affects aggregation processes with the competitive occurrence of different growth mechanisms.

This overall behavior can be attributed to the role of two main parameters at the basis of soot formation processes: the soot induction delay time and the concentration level of soot precursors. Further investigation is required to gain a deeper insight in this direction.

References

1. Ö.L. Gülder, D.R. Snelling, R.A. Sawchuck, Proc. Combust. Inst. **26**, 2351 (1996)
2. P.A. Tesner, Proc. Combust. Inst. **7**, 546 (1958)
3. M. Karbasi, I. Wierzba, Int. J. Hydrog. Energy **2**, 123 (1998)
4. A.R. Choudhuri, S.R. Gollahalli, Int. J. Hydrog. Energy **25**, 451 (2000)

5. R.W. Schefer, Int. J. Hydrog. Energy **28**, 1131 (2003)
6. F. Cozzi, A. Coghe, Int. J. Hydrog. Energy **31**, 669 (2006)
7. G. Yu, C.K. Law, C.K. Wu, Combust. Flame **63**, 339 (1986)
8. G.S. Jackson, R. Sai, J.M. Plaia, C.M. Boggs, K.T. Tiger, Combust. Flame **132**, 503 (2003)
9. F. Halter, C. Chauveau, I. Gokalp, Int. J. Hydrog. Energy **32**, 2585 (2007)
10. C. Tseng, Int. J. Hydrog. Energy **27**, 699 (2002)
11. M. Ilbas, I. Yilmaz, Y. Kaplan, Int. J. Hydrog. Energy **30**, 1139 (2005)
12. H. Guo, F. Liu, G.J. Smallwood, O.L. Gulder, Combust. Flame **145**, 324 (2006)
13. D.X. Du, R.L. Axelbaum, C.K. Law, Combust. Flame **102**, 11 (1995)
14. S. De Iuliis, S. Maffi, F. Cignoli, G. Zizak, Appl. Phys. B **102**, 891 (2011)
15. S. De Iuliis, A shock tube and burner study on soot growth rate from ethylene in presence of hydrogen by different optical diagnostics, Ph.D. thesis, Université d'Orleans, 22nd Cycle 2010
16. S. De Iuliis, F. Cignoli, S. Benecchi, G. Zizak, Appl. Opt. **37**, 7865 (1998)
17. R. Botet, R. Jullien, Ann. Phys. **13**, 153 (1988)
18. R.J. Samson, G.W. Mulholland, J.W. Gentry, Langmuir **3**, 272 (1987)
19. R.D. Mountain, G.W. Mulholland, Langmuir **4**, 1321 (1988)
20. U.O. Koylu, G.M. Faeth, T.L. Farias, M.G. Carvalho, Combust. Flame **100**, 621 (1995)
21. U.O. Koylu, C.S. McEnally, D.E. Rosner, L.D. Pfefferle, Combust. Flame **110**, 494 (1997)
22. F. Migliorini, S. De Iuliis, F. Cignoli, G. Zizak, Combust. Flame **153**, 384 (2008)
23. D. Bradley, K.J. Matthews, J. Mech. Eng. Sci. **10**, 299 (1968)
24. F. Migliorini, Study of combustion process of hydrogen-hydrocarbon mixtures, Ph.D. thesis, Dipartimento di Chimica Materiali e Ingegneria Chimica "Giulio Natta", Politecnico di Milano, XXI ciclo 2006–2008
25. C.S. McEnally, U.O. Koylu, L.D. Pfefferle, D.E. Rosner, Combust. Flame **109**, 701 (1997)
26. A.D. Abid, N. Heinz, E.D. Tolmachoff, D.J. Phares, C.S. Campbell, H. Wang, Combust. Flame **154**, 775 (2008)
27. B. Zhao, K. Uchikawa, H. Wang, Proc. Combust. Inst. **31**, 851 (2007)
28. U.O. Koylu, Y. Xing, D.E. Rosner, Langmuir **11**, 4848 (1995)
29. C.M. Sorensen, Aerosol Sci. Technol. **35**, 648 (2001)
30. A.M. Brasil, T.L. Farias, M.G. Carvalho, U.O. Koylu, J. Aerosol Sci. **32**, 489 (2001)
31. S. De Iuliis, F. Migliorini, F. Cignoli, G. Zizak, Appl. Phys. B, Lasers Opt. **83**, 397 (2006)
32. S.C. Graham, J.B. Homer, J.L.J. Rosenfeld, in *10th Int. Shock Waves Symposium* (1975), p. 621
33. T.T. Charalampopoulos, H. Chang, Combust. Sci. Technol. **59**, 401 (1988)
34. S.S. Krishnan, K.-C. Lin, G.M. Faeth, J. Heat Transf. **122**, 517 (2000)
35. M. Frenklach, Proc. Combust. Inst. **22**, 1075 (1989)
36. M. Frenklach, T. Yuan, M.K. Ramachandra, Energy Fuels **2**, 462 (1988)